# Design and analysis of a foldable / unfoldable corrugated architectural curved envelop

Francesco Gioia, David Dureisseix, René Motro, Bernard Maurin

# Design and analysis of a foldable / unfoldable corrugated architectural curved envelop

Francesco Gioia[*], David Dureisseix[†], René Motro[‡] and Bernard Maurin[§]

## Abstract

*Origami and paperfolding techniques may inspire the design of structures that have the ability to be folded and unfolded: their geometry can be changed from an extended, servicing state to a compact one, and back-forth. In traditional Origami, folds are introduced in a sheet of paper (a developable surface) for transforming its shape, with artistic or decorative intent; in recent times the ideas behind origami techniques were transferred in various design disciplines to build developable foldable / unfoldable structures, mostly in aerospace industry [19, 16]. The geometrical arrangement of folds allows a folding mechanism of great efficiency and is often derived from the buckling patterns of simple geometries, like a plane or a cylinder (e.g. Miura-Ori and Yoshimura folding pattern) [29, 15]. Here we interest ourselves to the conception of foldable / unfoldable structures for civil engineering and architecture. In those disciplines, the need for folding efficiency comes along with the need for structural efficiency (stiffness); for this purpose we will explore nondevelopable foldable / unfoldable structures: those structures exhibit potential stiffness because, when unfolded, they cannot be flattened to a plane (non-developability). In this paper we propose a classification for foldable / unfoldable surfaces that comprehend non fully developable (and also non fully foldable) surfaces and a method for the description of folding motion. Then we propose innovative geometrical configurations for those structures by generalizing the Miura-Ori folding pattern to non-developable surfaces that, once unfolded, exhibit curvature.*

*This is a preprint of an article that was published in its final form in* Journal of Mechanical Design*, Volume 134, Issue 3, March 2012, Pages 031003. doi: 10.1115/1.4005601*

[*]Dipartimento di Architettura, Costruzioni e Strutture (DACS), Università Politecnica delle Marche, Ancona, Italy I-60121, Email: francescogioia@email.it

[†]Contact and Structural Mechanics Laboratory (LaMCoS), INSA de Lyon / CNRS UMR 5259, Villeurbanne, France F-69621, Email: David.Dureisseix@insa-lyon.fr

[‡]Mechanics and Civil Engineering Laboratory (LMGC), University Montpellier 2 / CNRS UMR 5508, Montpellier, France F-34095, Email: Rene.Motro@univ-montp2.fr

[§]Mechanics and Civil Engineering Laboratory (LMGC), University Montpellier 2 / CNRS UMR 5508, Montpellier, France F-34095, Email: Bernard.Maurin@univ-montp2.fr

## 1 Introduction

Man-made objects that present folds and corrugations may be more interesting than smooth ones: corrugations add a tactile dimension and increase the three-dimensional perception. The morphogenetic processes in nature form folds and corrugation, for either structural or functional reasons, sometimes resulting in expressive shapes [5]. In design disciplines, the manipulation of a folded sheet allows to experience directly the relation between geometry and rigidity, and, as recognized at the Bauhaus in the 20's, the fold is also a powerful design method. In contemporary architecture, the fold is described in different ways: as a morphogenetic process, as a structural rib, and as a mean to realize deployable envelops, Figure 1. We will consider this third case, as foldable / unfoldable structural systems are of importance, in civil engineering and architecture, to design temporary structures or convertible roofing. Other technologies allow as well such abilities, for instance:

- Tensegrity structures (with cables and bars) [11],
- Textile and / or inflatable structures [22],
- Panels and hinges as particular mechanisms [12, 25]

or possible hybrid structures, associating two or several of the previous solutions.

This article focuses on the case of panel and hinge mechanisms, inspired with paperfolding techniques (origami), and we restrict ourselves to thin planar panels assumed to be kept planar during the folding / unfolding movement. The case of mechanisms with one degree of mobility is particularly under concern.

The aim of this study is first to propose a classification and description of such systems, potentially not fully developable to exhibit potential stiffness, for design choice purposes rather than merely for analysis of existing solutions. Second, we propose geometrical models for non-developable foldable / unfoldable surfaces: The detailed designed surface is not prescribed to be planar, and the average surface of the overall unfolded structure may exhibit curvature. The resulting structures will be called *foldable corrugated meshes*. In order to help the fabrication process, the surfaces are composed as much as possible of identical units and plates. Therefore, the increase in complexity for designing these surfaces only lies in a larger number of types of planar elementary plates to be produced (typically 2 types of plates, compared to only one for classical Miura-Ori).

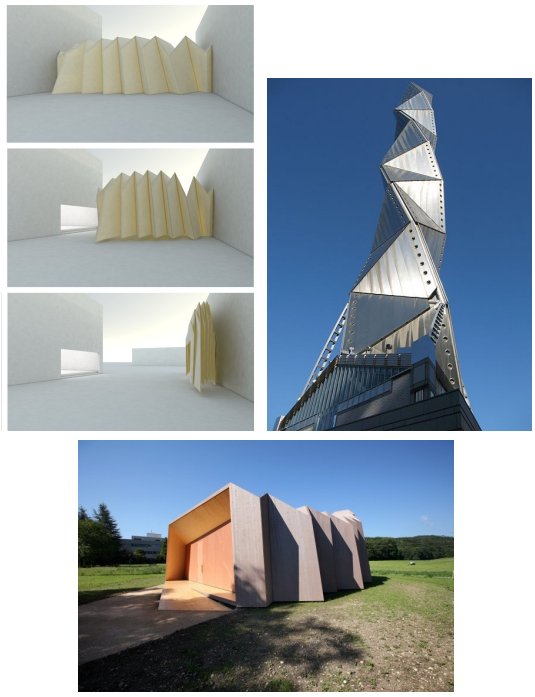

Figure 1: Using folds in architecture. Top left: kinematic aspect of a foldable gallery (T. Tachi [26]); top right: morphogenetic aspect of the Art Tower Mito (A. Isozaki, image by Korall, Creative Commons 2006); bottom: static aspect for the Saint Loup Chaptel (Localarchitecture / H. Buri, Y. Weinand / D. Mondada, 2008 [1])

## 2 Geometrical surfacic description

Since the targeted surfaces are only piecewise differentiable, they are not smooth surfaces and tangential planes cannot be defined everywhere. By analogy with 'rigid folding' in origami and 'rigid theory' [7] in mechanism analysis [23, 9], we neglect the thickness of the plates which are one-to-one connected with perfect hinges. The plates themselves are delimited either with the total structure edges, or by their hinges. All plates are assumed to be kept planar and the edges are straight segments, [24]. Note that more generally, the plates could be considered as developable surfaces [6, 8], if one models the bending of these surfaces (that can store bending elastic energy as a possible energy for actuation) ; such bendings are unavoidable if one uses curved creases to obtain a foldable / deployable system [3, 4, 17, 18]. This aspect is nevertheless not under the scope of the present study, for which the 'folds' are straight edge segments.

### 2.1 Orientation

A corrugated mesh is defined as a simply connected surface composed of planar polygonal faces. The neighboring relations are established between adjacent faces along folding edges, i.e. the shared edges of two faces. We assumed that such a surface is orientable, i.e. a continuous orientation can be defined for each face $F_i$, $i = 1, \dots n$, by assigning its normal unitary vector $\underline{n}_i$. Each face $F_i$ is composed of $k_i$ vertices $V_i^j$, $j = 1, \dots k_i$, and $k_i$ edges $\underline{E}_i^j$ that can be numbered counterclockwise with respect to the normal vector $\underline{n}_i$, see Figure 2. In such a case, $\underline{E}_i^j = V_i^{(j \bmod k_i)+1} - V_i^j$.

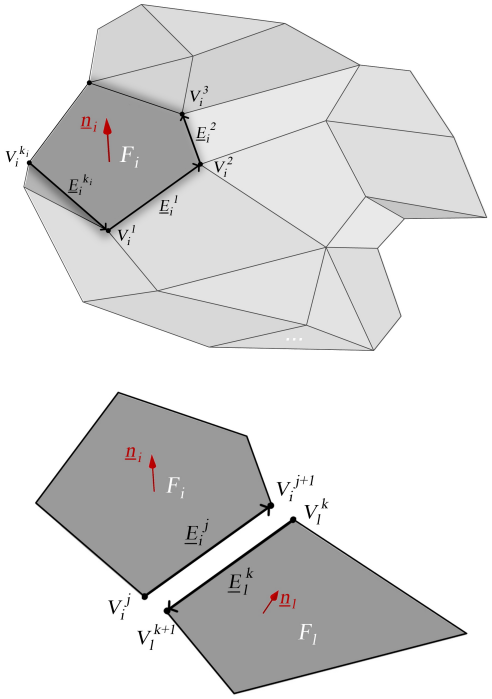


Figure 2: Definition of a configuration and orientation of its surface

Additionally, the $k_i$ sector angles between two adjacent edges are defined for each face $F_i$ with angles $\theta_i^j = \angle(\underline{E}_i^j, \underline{E}_i^{(j \bmod k_i)+1})$, for $j = 1, \dots k_i$. $0 \leq \theta_i^j \leq 2\pi$, since edges are oriented.

With an orientable overall plate assembly $\Omega = \cup_{i=1}^n F_i$, if the edge $j$ of face $F_i$ is shared with the edge $k$ of a neighboring face $F_l$, then (Figure 2): $\underline{E}_i^j = -\underline{E}_l^k$. We finally assume that two faces share at most one straight folded edge; when two neighboring faces share one edge, their common edge is denoted with $\underline{e}_{il} = \underline{E}_i^j = -\underline{E}_l^k$.

### 2.2 Folding angles

The angle between two normals of adjacent faces is $a_{il} = \arccos(\underline{n}_i \cdot \underline{n}_l)$, and $0 \leq a_{il} \leq \pi$. These angles, as well as their corresponding edges $\underline{e}_{il}$ are split into two groups: If we denote the external side of the overall surface as the side toward which all the normals are pointing to (see Figures 3 and 4), the neighboring faces which form a convex (respectively concave) dihedral, with respect to the external side, share a common edge called mountain (respectively valley) fold.

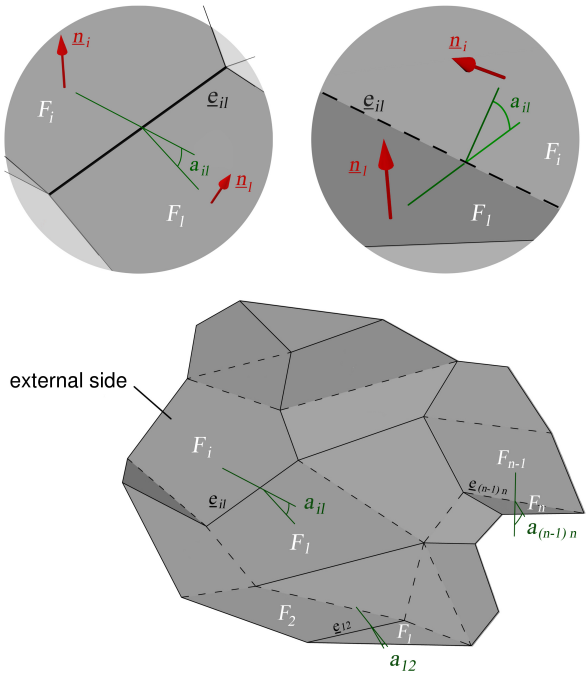


Figure 3: Mountain fold (upper left, denoted with straight lines) and valley fold (upper right, denotes with dotted lines)

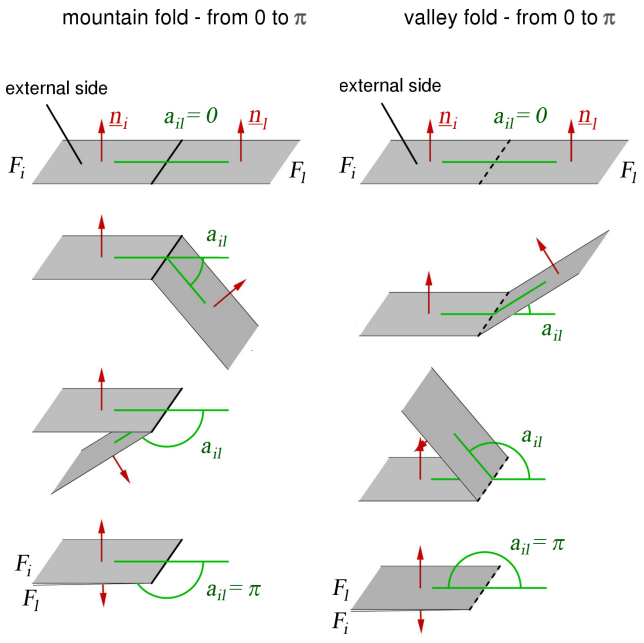


Figure 4: Possible evolutions of folds during folding movement, and local folding angle

# 3 Foldability

The global foldability along an entire path, i.e. a set of successive states of the corrugated mesh $\Omega$ when changing continuously the folding angles but preserving planarity of each face, edge connections, and avoiding face interpenetration, is still an open question. Nevertheless, the so-called local foldability condition (a necessary condition) can be stated close to each fold intersection $O$ (or corner node), Figure 5 (left), i.e. at each end point common to several common edges as [7]:

$$p \text{ is even, and } \sum_{m=1}^{p} (-1)^m \theta_m \in \{0, 2\pi, -2\pi\} \qquad (1)$$

if, without loss in generality, we number consecutively the faces according to the global orientation as $m = 1, \dots p$ and concerned sector angles as $\theta_m$ around the point $O$. The sum is therefore performed on the faces that share the fold intersection $O$. If a flat configuration is possible, i.e. if $\sum_{m=1}^{p} \theta_m = 2\pi$ (developed state for which $\forall ij,\ a_{ij} = 0$) this condition is equivalent to: $p$ is even and $\sum_{m=1}^{p} (-1)^m \theta_m = 0$; but it is also valid for cases where the overall sum is greater or smaller that $2\pi$ [7], Figure 5. In such cases, no fully developed state exist.

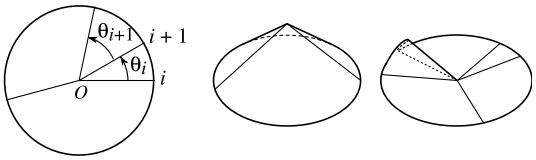


Figure 5: Illustration of local flat foldability, for the flat unfolded state (left), and two non-flat states (center and right)

The local foldability condition is a necessary, but not a sufficient condition to the existence of a flat folded state ($\forall ij,\ a_{ij} = \pi$). Indeed, for the assembly of rigid plates and perfect hinges to exhibit a finite mechanism, persistent compatibility of rotation rates $\dot{a}_{ij}$ and global non penetrability conditions are additionally required. If it is the case (i.e. if the corrugated mesh is foldable), the configuration $\Omega$ may evolve with an external null energy driving. Eventually, during this motion, mountain folds may transform into valley folds, and reverse (when an $a_{ij}$ is close to 0, but not close to $\pi$ due to non penetration condition). The set of these continuously successive configurations is called the folding path.

It should be noted that the foldability requirement is a strong constraint on the design of the plate assembly.

## 3.1 Folded and unfolded states

To describe the possible variations of the folding angles, and the admissible path of the corresponding configurations during a folding or unfolding operation, we propose a global descriptor $G_\Omega$ for an admissible state $\Omega$ as

$$G_\Omega = \frac{1}{q} \sum_{ij} \frac{a_{ij}}{\pi} \qquad (2)$$

where $q$ is the number of common edges $\underline{e}_{ij}$ and of folding angles $a_{ij}$. Since $0 \leq a_{ij} \leq \pi$, one gets $0 \leq G_\Omega \leq 1$. $G_\Omega = 0$ corresponds to have all faces coplanar ($\forall ij,\ a_{ij} = 0$, this is the developed state); $G_\Omega = 1$ corresponds to have all faces overlapping ($\forall ij,\ a_{ij} = \pi$, this is the flat-folded state).

This global descriptor allows to define the unfolded state $\Omega'$ as the state that minimizes the value of $G_\Omega$ over the set of all the admissible states (the total folding path): $\forall \Omega,\ G_{\Omega'} \leq G_\Omega$; the state $\Omega''$ that maximizes this value will be called the folded state: $\forall \Omega,\ G_{\Omega''} \geq G_\Omega$. If there exist only one continuous path between an unfolded and a folded state, the foldable corrugated mesh has a unique folding path, Figure 6, otherwise, it has multiple folding paths.

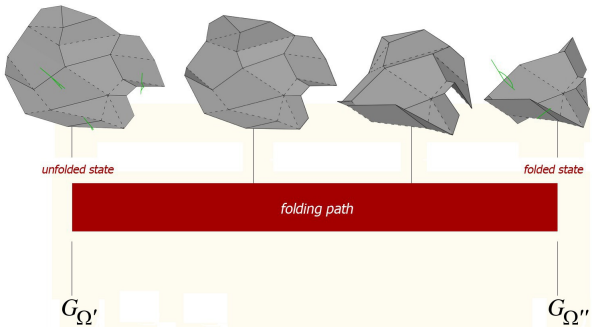


Figure 6: Global descriptor $G_\Omega$ as the parameter of a unique folding path ($G_{\Omega'} \leq G_\Omega \leq G_{\Omega''}$)

## 3.2 Folding path and classification

The description of the folding path is quite explicit when using the evolution of the configuration along with the values of $G_\Omega$. Extremal reachable values allow to define:

- A developable corrugated mesh: the unfolded state is planar, $G_{\Omega'} = 0$;
- A non-developable corrugated mesh: $G_{\Omega'} > 0$;
- A flat-foldable corrugated mesh: the folded state is planar, $G_{\Omega''} = 1$;
- A non flat-foldable corrugated mesh: $G_{\Omega''} < 1$;

and four different combinations of these cases are possible. Moreover, the case where $G_{\Omega'} = G_{\Omega''}$ corresponds to an unfoldable (or rigid) corrugated mesh. Figure 7 recalls and compares the different possibilities, with examples of corrugated meshes.

$G_\Omega$ is a useful intrinsic characteristic of a configuration $\Omega$ that leads to smooth evolutions of folding angles. Nevertheless, it may be difficult from a control point of view to command the folding / unfolding movement with $G_\Omega(t)$: It would correspond to exert an identical torque on every hinge simultaneously. A small modification of the definition of $G_\Omega$ consists in using the squared values $(a_{ij}/\pi)^2$, that corresponds to elastic rotational springs at each

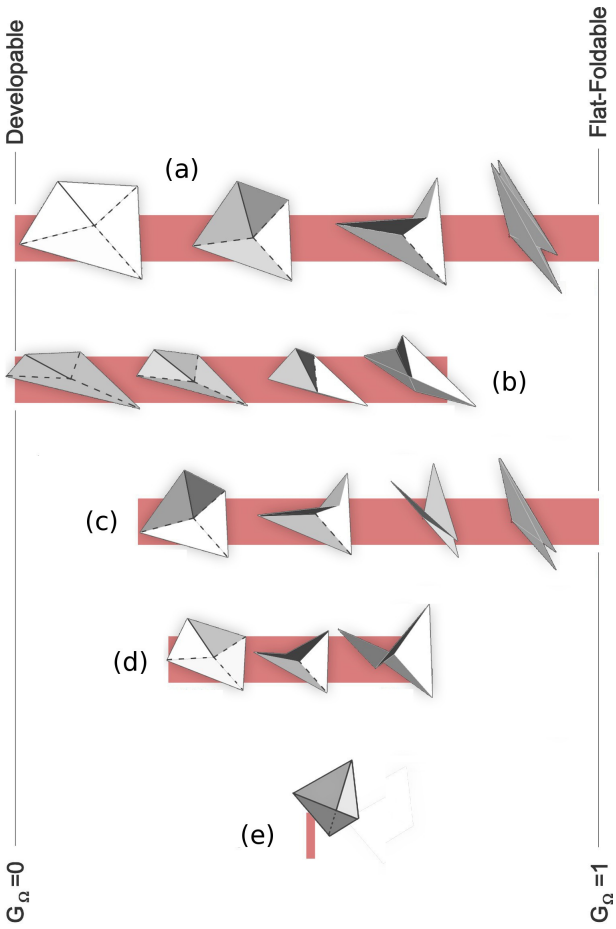


Figure 7: Classification and examples of foldable corrugated meshes; (a) developable and flat-foldable, (b) developable and non flat-foldable, (c) non developable and flat-foldable, (d) non developable and non flat-foldable, (e) unfoldable (rigid)

hinge. In such a case, these elastic springs would store the actuation energy, useful for deployment. The fact that the use of $G_\Omega$ (present, or with squared values) as a folding path parameter leads to smooth curves for the evolution of folding angles explains why systems with such elastic springs to store actuation energy may easily deploy themselves with a low probability of locking [2]. An other command would focus on one or few rotation angles $a_{ij}$. To check commandability, one can plot the evolution of the corresponding rotation angles with respect to $G_\Omega$, as in Figure 8. With a non-univoque relationship (as for curve 1 in Figure 8) the deployment cannot be entirely controlled. Indeed the dead center (the velocity inversion point) separates the path into two sub-paths. Unless an additional actuator (even for a mechanism with one mobility) is added to a rotation angle that does not posses a dead center at the same location (or using dynamical effects to pass through the dead center, which is not a reliable command), the two sub-paths are separated.

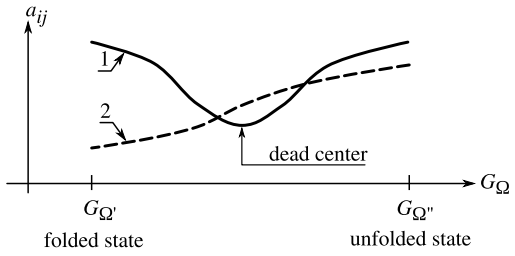


Figure 8: Controlability of folding path: typical evolution of two degrees of freedom versus $G_\Omega$

# 4 A case study: Generalized Miura-Ori surface

We propose herein a geometrical model of a foldable corrugated mesh which is a generalization of the Muira-Ori origami surface [21, 20], a developable and flat-foldable corrugated mesh, whose unfolded state can tessellate a plane. It has a unique folding path with a great packaging efficiency that makes it useful for deployable planar structures. However, for the design of foldable / unfoldable architecture envelops (structures that demands both packaging efficiency and stiffness), it lacks of structural rigidity, since the unfolded state is a plane (developable corrugated mesh), a surface with no out-of-plane stiffness. The proposal is therefore to modify geometrically the Miura-Ori fold in order to prevent its unfoldability to a plane, and additionally to approximate non-planar average surfaces.

There exist many generalizations of Miura-Ori fold approximating three-dimensional non planar surfaces, [12, 25] for instance, see Figure 9. Though interesting from a geometrical standpoint, these surfaces do not achieve structural efficiency, since they keep being developable corrugated meshes: the non-planar surface is approximated in an intermediate (geometrically changing due to mechanisms) state during the folding path, and do not exhibit stiffness. Some non-developable units nevertheless exists [27] but cannot be assembled into larger one-degree-of-mobility corrugated meshes unlike the developments presented herein.

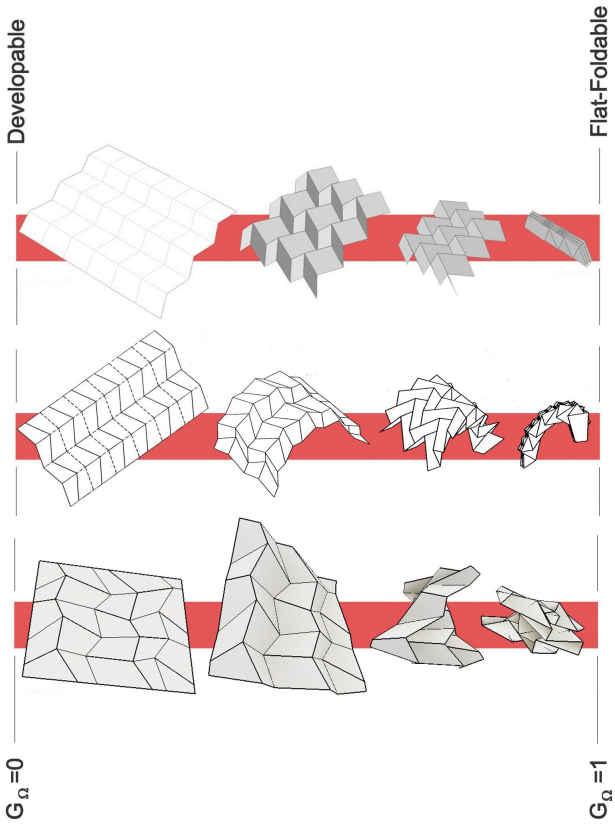


Figure 9: Examples of Miura-Ori generalizations; top: genuine Miura-Ori fold; middle: Curved pleated sheet structure [12]; bottom: Generalization of quadrilateral mesh origami [25]

The aim of our generalization is to modify the geometry of the Miura-Ori fold in order to prevents its developability while keeping its kinematic efficiency (i.e. to preserve its ability to easily unfold from a very compact folded state to a wide area coverage unfolded state), to get a non-developable and flat-foldable corrugated mesh. The unfolded state then tessellates a 'thick' plane, so we can define its thickness, and its folding path spreads from this thick plane state to a completely flat-folded state. With further geometrical modifications, this corrugated mesh can approximate single-curved surfaces, thus tessellating thick cylinders, increasing stiffness and keeping flat-foldability.

## 4.1 Miura-Ori

This wide-known developable and flat-foldable corrugated mesh is composed of repetitive rhombuses that tessellate a plane Figure 9 (top). The rhombuses are defined by an angular parameter $\alpha$ and the edge length $l$. Its analysis can be derived from a single basic unit, Figure 10, on which the sector angles surrounding every fold

intersection are: $\theta_1 = \theta_4 = \alpha$, $\theta_2 = \theta_3 = \pi - \alpha$, therefore satisfying the local foldability condition (1), and the developability condition (the sector angles sum to $2\pi$).

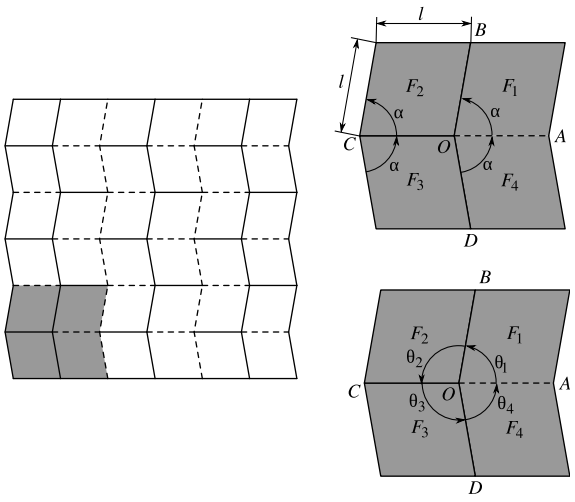


Figure 10: Foldability properties of the Miura-Ori tessellation (straight lines are mountain folds, dotted lines are valley folds)

If we apply a kinematic constraint (for example when decreasing the distance between vertices $A$ and $C$), Figure 11, a finite mechanism is activated, and, according to [14, 13], there exists a one-to-one map between the folding angles: $a_{41} = a_{23}$ and $a_{12} = a_{34}$. Therefore, the folding path of the basic unit can be completely described with a single parameter once the design parameter $\alpha$ has been chosen. This path is depicted on Figure 12.

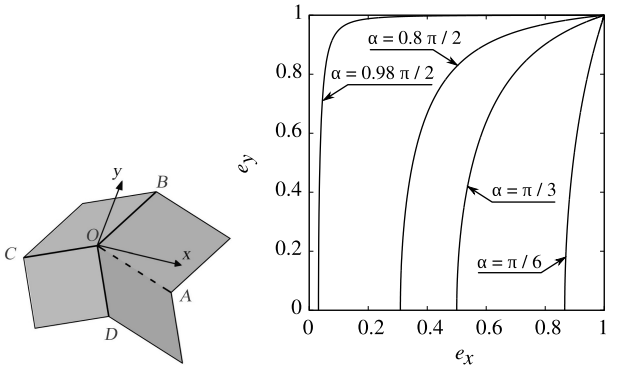


Figure 11: Characteristics of the Miura-Ori basic unit: Expansion coefficients along $x$ and $y$ directions: $e_x$ and $e_y$

Several characteristics of the basic unit may be drawn. For instance, the evolution of the folding angles with $G_\Omega$, but also the expansion coefficients [21]: If the unit is confined between two external tangent planes, parallel to $\underline{CA}$ and $\underline{DB}$, as in Figure 11, the unit deployment happens simultaneously in two orthogonal directions (lying in the tangent planes and respecting symmetries) $x$ and $y$; the expansion coefficient $e_x$ (respectively $e_y$) is the ratio of the length of segment $CA$ (respectively $DB$) and their respective maximum values.

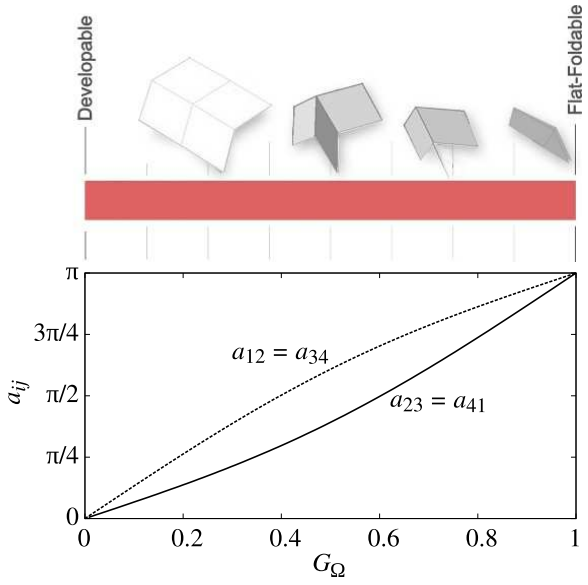


Figure 12: Folding path for the Miura-Ori basic unit

The modified basic unit we propose hereafter should preserve these properties, while leading to a non-developable corrugated mesh in order to exhibit stiffness for the unfolded state.

## 4.2 Generalized unit and folding path

In a basic unit of the Miura-Ori surface, the four sector angles sum up to $2\pi$; we propose to modify two of them to sum to more than $2\pi$, Figure 13. These four sector angles are now: $\theta_1 = \theta_4 = \alpha + \beta$, $\theta_2 = \theta_3 = \pi - \alpha$. They still satisfy the local foldability condition (1), but no more the developability condition since their sum is $\sum_m \theta_m = 2\pi + 2\beta$. On such a simple fold, the local non penetration condition during folding process can be derived: $\theta_1 \geq \theta_2$, resulting in restriction range for $\beta$: $\beta \leq \pi - 2\alpha$.

If we scale up the model to $l = 1$ to simplify the expressions, without loss in generality in all of the following, and choose a coordinate orthonormal basis $(\underline{x}', \underline{y}', \underline{z}')$ such that $\underline{x}' = \underline{CO}$, $\underline{y}'$ lies in $F_2$ and is close to $\underline{OB}$ as for a Gram-Schmidt orthonormalization of $(\underline{CO}, \underline{OB})$, Figure 13(d), the vector $\underline{OA}$ is obtained by rotation of an angle $a_{12}$ of vector $\begin{bmatrix}\cos\beta & -\sin\beta & 0\end{bmatrix}^T$ along $\underline{OB} = \begin{bmatrix}\cos\alpha & \sin\alpha & 0\end{bmatrix}^T$. After trigonometric developments, this leads to its coordinates as functions of $a_{12}$:

$$x_A = \cos a_{12}\sin\alpha\sin(\alpha+\beta) + \cos\alpha\cos(\alpha+\beta) \quad (3)$$

$$y_A = -\cos a_{12}\cos\alpha\sin(\alpha+\beta) + \sin\alpha\cos(\alpha+\beta) \quad (4)$$

$$z_A = -\sin a_{12}\sin(\alpha+\beta) \quad (5)$$

A compatible state satisfies to $A = A'$. Due to the symmetry plane of normal vector $\underline{n} = \begin{bmatrix}0 & \cos(a_{23}/2) & \sin(a_{23}/2)\end{bmatrix}^T$, this condition also means that $A$ lies in the symmetry plane, i.e. $\underline{OA}\cdot\underline{n} = 0$. This relation links the two kinematic parameters $a_{12}$ and $a_{23}$ as a

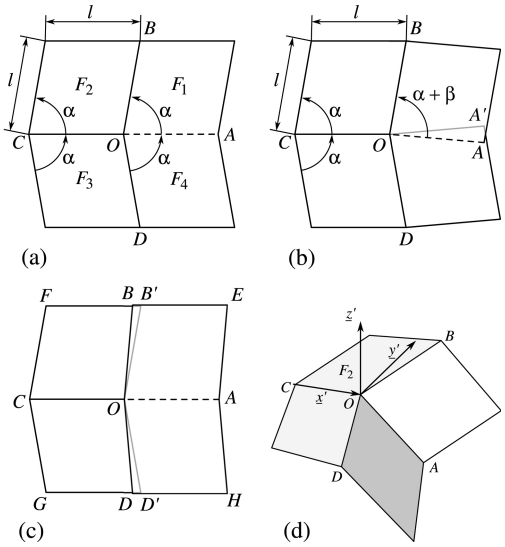


Figure 13: Modification of the Miura-Ori basic unit to a non-developable corrugated unit (straight lines are mountain folds, dotted lines are valley folds); (a) original Miura-Ori unit, (b) modified unit, (c) another assembly process of the same modified unit, (d) dedicated coordinate basis for the analysis

continuous map that describes admissible states:

$$\tan(a_{23}/2) = -y_A/z_A \tag{6}$$

Finally, $a_{41}$ can be obtained with $a_{41} = \arccos(\underline{n_4} \cdot \underline{n_1})$. An other assembly process consists in noting that the generalized unit can be assembled along edges $OD$ and $OC$, Figure 13 (c). In such a way, one gets for the assembled admissible state $\angle(\underline{CG}, \underline{CF}) = \angle(\underline{OD}, \underline{OB}) = \angle(\underline{AH}, \underline{AE})$ which leads to the following expression:

$$\cos a_{41} = \frac{\cos^2(\alpha+\beta) - \cos^2\alpha + (\sin^2\alpha)\cos a_{23}}{\sin^2(\alpha+\beta)} \tag{7}$$

For feasible ranges of design parameters $\alpha$ and $\beta$, expression (6) is a monotone relationship, and for $a_{23} \in [0, \pi]$, one gets $a_{12} \in [a''_{12}, \pi]$ where the minimal value $a''_{12}$ is obtained from (6): $\cos a''_{12} = \tan\alpha/\tan(\alpha+\beta)$. The unfolded state therefore corresponds to $a_{12} = a''_{12}$ and $a_{23} = 0$.

The folding motion is therefore described with a unique parameter, and the unit has a unique folding path, depicted on Figure 14 (for $\alpha = \pi/3$ and $\beta = \pi/10$). This is therefore the proof that the proposed unit is a mechanism with a single degree of mobility.

## 4.3 Generalized unit characteristics

As for the Miura-Ori basic unit and assembly, the expansion coefficients on the two orthogonal directions $x$ and $y$ can be defined. Their evolutions along the folding path now depend on the two design parameters $\alpha$ and $\beta$. An interesting angle is $\xi = \angle(\underline{OC}, \underline{OA})$ with $\cos\xi = \underline{OC} \cdot \underline{OA} = -x_A$. For the unfolded state this value is

$$\cos\xi'' = -\cos(\alpha+\beta)/\cos\alpha \tag{8}$$

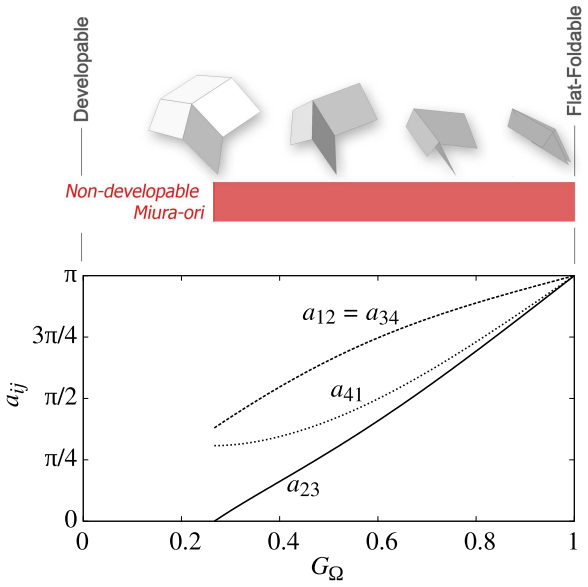


Figure 14: Folding path for the non-developable unit

Then, one gets $CA = 2\sin(\xi/2)$ and $DB = 2\sin\alpha\cos(a_{23}/2)$, so the expansion coefficients are $e_x = \sin(\xi/2)/\sin(\xi''/2)$ and $e_y = \cos(a_{23}/2)$

The evolutions of these two expansion coefficients from folded to unfolded state are plotted in Figure 15 for different values of $\alpha$ and $\beta$. Increasing $\alpha$ allows a larger variation of the $e_x$ coefficient. For $\alpha \to \pi/2$, these co-evolution curves tend to two orthogonal segments, i.e. two decoupled movements, with difficulties in the command control.

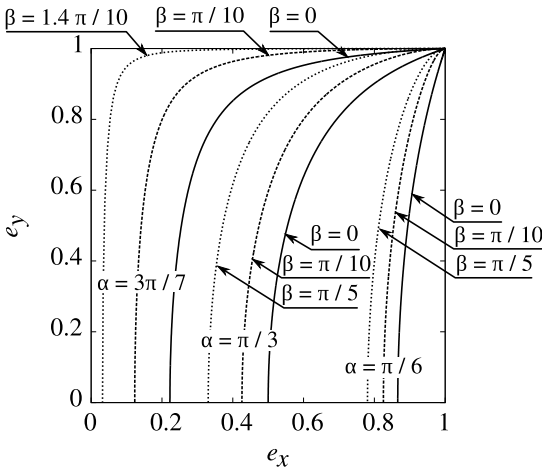


Figure 15: Expansion coefficients for different design parameters

Another characteristic is the 'thickness' of the average surface of the unfolded state, Figure 16: $t = (1+\cos\alpha)\cos(\xi''/2)$. This thickness describes the non-planarity of the unfolded state, and is related to structural efficiency: increasing the thickness also increases the quadratic moments of the average surface (the coeffi-

cients in the strength and in the stiffness expressions of a 'thick' surface that arise from geometry and not from material characteristics), and consequently its load-bearing capacity.

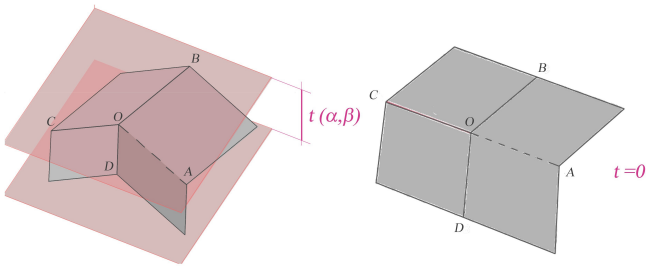


Figure 16: Thickness of the unfolded state of the non-developable unit (left) and of the Miura-Ori unit (right, with zero thickness)

Figure 17 (left) shows a plot of the values of this thickness. Although for $\alpha = \pi/4$ and $\beta = \pi/2$ the thickness is maximum, for those design values, the surface covered (projected to $(x, y)$ plane) is relatively small, Figure 17 (right). This projected surface is given with: $A = 4\sin(\xi''/2)$. Depending on the application, a compromise should be made; for instance, Figure 18 shows plots of the product of the thickness with the covered area $t(\alpha, \beta) \times A(\alpha, \beta)$. It allows for instance, to maximize this equivalent volume on design parameters.

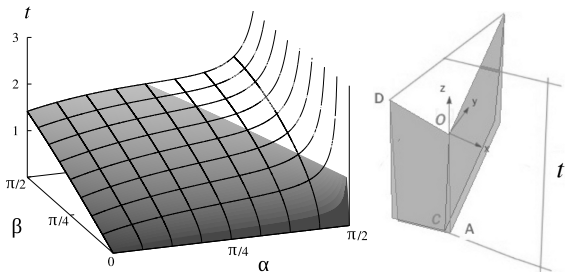


Figure 17: Evolution of the thickness with design parameters (left, lighter color: not admissible states), folded state for the maximal thickness (right)

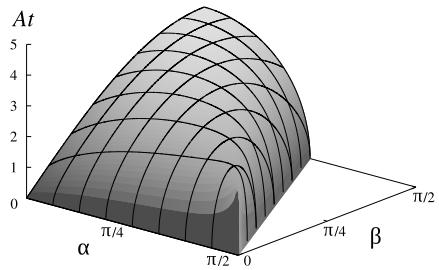


Figure 18: Product of the thickness with the covered area of the unfolded state

## 4.4 Unit assembly

As already stated, all along the folding path, two opposite sides of the unit have the same folding angle. Moreover, considering again the assembly process of Figure 13 (c), the edges of the plates are parallel and stay parallel all along the folding path. Therefore, the corner nodes of two opposite sides of the unit deduce themselves with a translation (of vector $\underline{CA}$ for one side, and $\underline{DB}$ for the other one). Thanks to these properties, the basic units can be assembled in two directions, either $x$ or $y$, in a modular array. With periodic translations along these directions, the whole thick plane can be tessellated, and the unit characteristics pertain to the assembly: a unique folding path, a mechanism with a unique degree of freedom, non-developability, flat-foldability, evolutions of expansion coefficients and thickness. The deployment still happens simultaneously in two orthogonal directions and is allowed from a compact flat-folded state (packing efficiency) to an extended predetermined service state (unfolded state), and back-forth (folding), following the same path. Figure 19 illustrates the folding path for a 3-by-3 array that was geometrically constructed in Grasshopper®, a graphical algorithm editor integrated with Rhino3D® modeling tools, allowing to draw parametrically-driven 3D geometries. The planes into which are located the boundary nodes of the basic units are kept plane all along the folding path. For this model, the input parameters are the angles $\alpha$, $\beta$, the edge dimension $l$ (scale of the model), and for describing the unique folding path, a kinematic parameter.

# 5 Single curved surface assemblies

To modify the geometry of the basic unit, and to lead to assemblies that approximate single-curved surfaces, we introduce an additional angular parameter, Figure 20. Since for the planar assembly we defined two sets of folding planes that remain parallel and mutually orthogonal during the folding path, for the single-curved assemblies, the sets of folding planes are now parallel for one set and radial for the other one, Figure 21. The new parameter may be either:

- $\gamma$ for obtaining an $y$-direction single curved surface, with a curvature radius $R_y$ and a circle sector angle $\kappa_y$;
- or $\delta$ for obtaining an $x$-direction single curved surface, with a curvature radius $R_x$ and a circle sector angle $\kappa_x$.

The resulting surfaces, depending on the sign of $\gamma$ or $\delta$, approximate concave or convex sectors of cylinder, Figure 21. They are still non-developable and flat-foldable corrugated meshes.

The design process for these surfaces is the following. Consider the juxtaposition of two identical units (with the same folding state) along one of the direction $x$ or $y$. Consider that each unit is assembled with infinite strips as faces, and rotate one of the unit of a global angle $\kappa$ along the other characteristic direction.

For the first type of surfaces (with $x$-curvature), the assembly of two units (with subscripts 0 and 1) initially by translation along

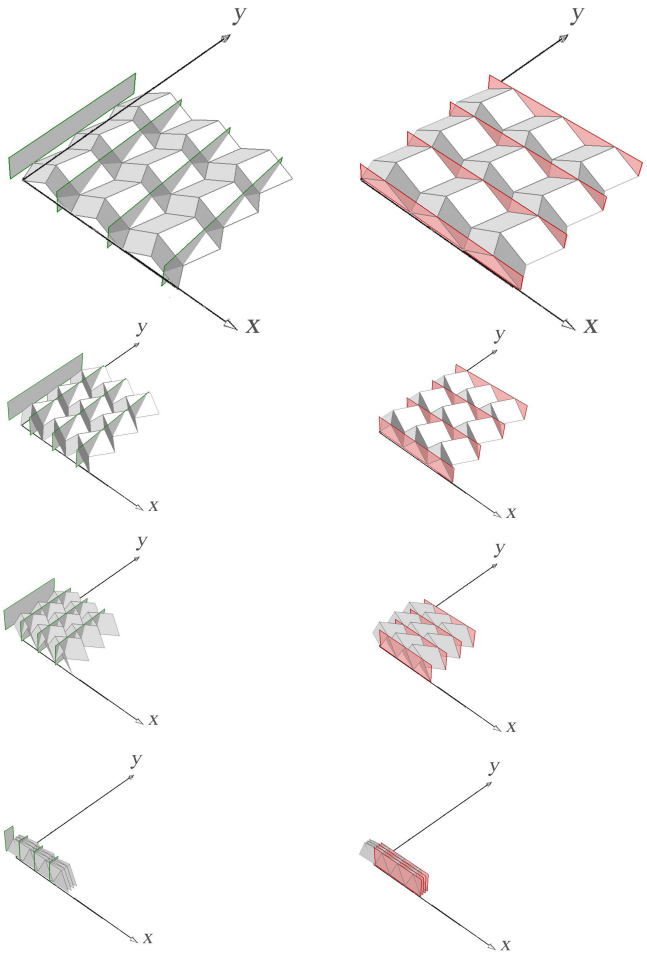


Figure 19: Folding path of a 3-by-3 unit assembly. Two arrays of orthogonal planes are conserved along the path

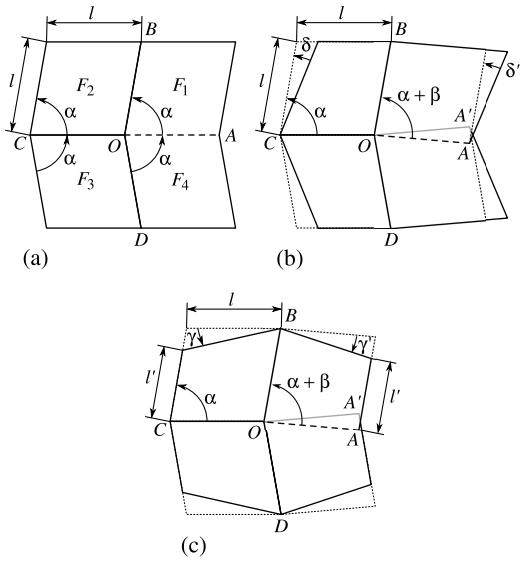


Figure 20: Modification of the Miura-Ori basic unit to a non-developable corrugated units with single curvature (straight lines are mountain folds, dotted lines are valley folds); (a) original Miura-Ori unit, (b) modified unit of first type ($x$-curved surface), (c) modified unit of second type ($y$-curved surface)

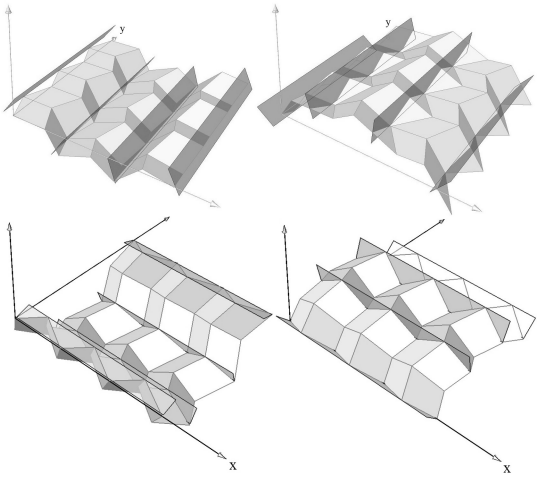


Figure 21: Four different 3-by-3 unit assemblies to get single-curved flat-foldable corrugated meshes. From left to right and top to bottom: concave $x$-curvature, convex $x$-curvature, concave $y$-curvature, convex $y$-curvature. Two arrays of orthogonal planes are conserved along the path; one being a radial array.

vector $\underline{CA}$, uses also a rotation of angle $\kappa_x$ along $\underline{DB}$ at point $A_0 = C_1$, Figures 22 and 23. Since the upper nodes are always located in the same plane (see Section 4.4), the corresponding faces of the two units intersect along $A_0E_0 = C_1F_1$ and $A_0H_0 = C_1G_1$, all segments having the same length. This 2-unit assembly gets useful information considering the local assembly of the former unit (with $\delta = \delta' = 0$, characterized with the design parameters $\alpha$ and $\beta$ and the folded state given for instance with angles $a_{23}$ and $\xi$) and of the new unit, whose characteristics are denoted with overlined quantities ($\bar{\alpha} = \alpha - \delta$, $\bar{\beta} = \beta + \delta - \delta'$, $\bar{a}_{23}$, $\bar{\xi}$), Figure 23. Therefore, (i) the angle $\delta'$ is directly obtained from $\delta$, providing identical length of segments $A_0E_0$ and $C_1F_1$; this assembly condition reads $\sin(\alpha+\beta)/\sin(\bar{\alpha}+\bar{\beta}) = \sin\alpha/\sin\bar{\alpha}$, that leads to

$$\delta' = \alpha + \beta - \frac{\pi}{2}\arccos\frac{\sin(\alpha+\beta)\sin(\alpha-\delta)}{\sin\alpha} \qquad (9)$$

N.B. (DD on 2012, 4 december) Is it a wrong formula? May be

$$\delta' = \alpha + \beta - \arcsin\frac{\sin(\alpha+\beta)\sin(\alpha-\delta)}{\sin\alpha}$$

(ii) the angle $\delta$ is directly obtained from the given unit folding state and the global angle $\kappa_x$, with the second assembly condition of the units: $\bar{a}_{23} = a_{23}$ (same local folded state). If one reverses the process, i.e. if considering a given folding state for the units, and a given design parameter $\delta$, the global angle $\kappa_x$ can be computed as well. Therefore, for a given value $\delta$, making the folding state of the units continuously changing renders the global angle $\kappa_x$ continuously changing as well (within an admissible range). As a consequence, the assembly is also a mechanism with one degree of mobility. An interesting state is the unfolded state $\Omega''$ for which $a_{23} = 0 = \bar{a}_{23}$. With the expression (8) for the modified unit, $\cos\bar{\xi}'' = -\cos(\bar{\alpha}+\bar{\beta})/\cos\bar{\alpha}$, the corresponding sector angle $\kappa_x''$ can be obtained, together with the curvature radius $R_x''$, Figure 23: $\kappa_x'' = \xi'' - \bar{\xi}''$ and $R_x'' = \sin(\xi''/2)/\sin(\kappa_x''/2)$. For $0 < \delta < \alpha/2$, one gets a convex surface (with respect to the external face), and for $\delta < 0$, subjected to $\sin(\alpha-\delta) < \sin\alpha/\sin(\alpha+\beta)$, the surface is concave.

Similar arguments can be used for the $y$-curved surfaces, with a permutation of assembling directions: The units are assembled with a rotation of angle $\kappa_y$ along $\underline{CA}$. For the unfolded state $\Omega''$ with $a_{23} = 0$, $DB = 2\sin\alpha$, and (Figure 24): $R_y'' = \sin\alpha/\sin(\kappa_y''/2)$. The relation between $\gamma$ and $\kappa_y''$ can be obtained as previously: $\underline{z}$ is the normal to both faces $F_2$ and $F_3$, Figure 13, for state $\Omega''$; therefore if $\underline{z}'$ is obtained from $\underline{z}$ with a rotation of angle $\kappa_y''$ along the direction of $CA$, i.e. $\begin{bmatrix}\cos(\xi''/2) & 0 & -\sin(\xi''/2)\end{bmatrix}^T$, then

$$\tan\gamma = -\underline{z}'\cdot\underline{x}/\underline{z}'\cdot\underline{y} = -\cos(\xi''/2)(1-\cos\kappa_y'')/\sin\kappa_y'' \qquad (10)$$

For $0 < \gamma < \alpha/2$, one gets a convex surface, and for $\gamma > 0$, the surface is concave.

Additionally, the angle $\gamma'$ and the fact that this mechanism has 1 degree of mobility can be established from the assembling condi-

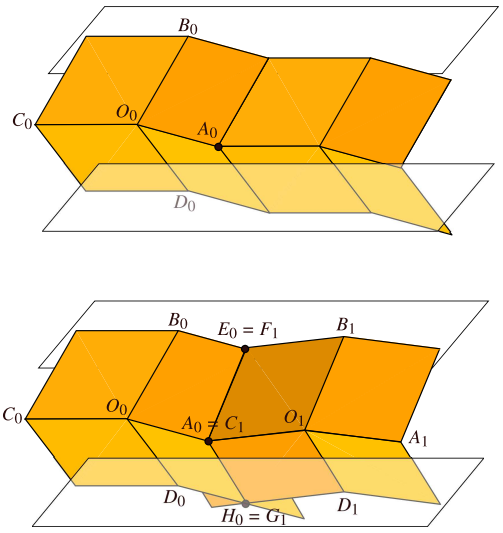


Figure 22: Design process for modifying the generalized unit to engender a curved global surface

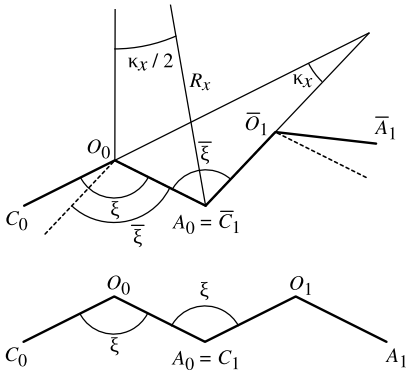


Figure 23: Assembly of two modified units for the second type of curved surface ($x$-cuved, within symmetry plane)

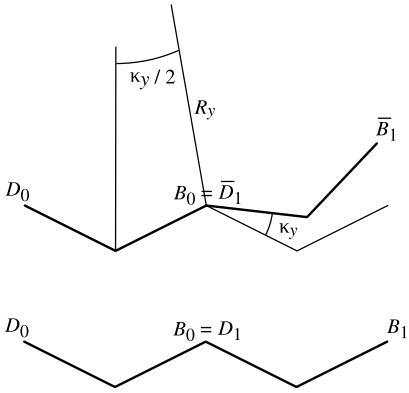


Figure 24: Assembly of two modified units for the first type of curved surface ($y$-curved, within the plane orthogonal to $\underline{CA}$)

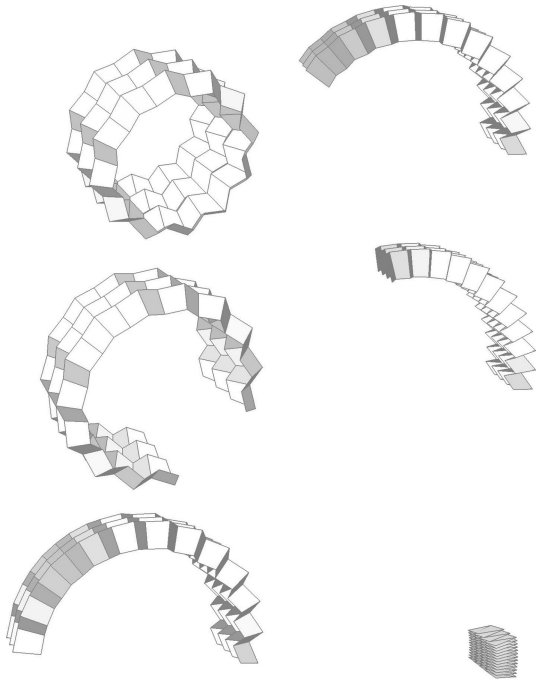

Figure 25: Convex $y$-curvature folding path

tion: $CF = AE$, that leads to

$$\tan\gamma' = \frac{\sin(\alpha+\beta)}{\sin\alpha/\tan\gamma - \cos\alpha - \cos(\alpha+\beta)} \tag{11}$$

Reversing the previous analytical relations between angular parameters and curvature radius, we can find, from a given basic unit with $\alpha$ and $\beta$ design values and from the desired curvature radius $R_y$ or $R_x$, the remaining design parameters $\gamma$ or $\delta$. With admissible values of curvature radius, we can tessellate four different thick cylinders. They are non-developable and flat-foldable corrugated meshes, with one degree of freedom folding motion. Several folding steps for three of the four different scenarios are presented in Figures 25 to 27. Nevertheless, the case of $x$-curvature cylinders are only locally foldable, since some faces self-intersect during the folding path. This illustrates that the local foldability conditions are not sufficient to ensure the global foldability or the non-penetration. Analytical developments are therefore useful for design and optimization purposes, and simulation can be used to check features such as global foldability with non-penetration requirements. Several ways to express necessary global foldability constraints may be found in [28] for instance, but up to now, only numerical approaches are available to check in a general and practical way the global non-penetration of non-adjacent plates.

The $y$-curvature cylinders do not exhibit such an interference, and Figure 28 illustrates a physical model of such a single curved assembly of 9 units, that has been built at the model laboratory of the École Nationale Supérieure d'Architecture de Montpellier, thanks to Dr. Arch. V. Raducanu, F. Gioia and N. Céleste, with piano hinges and 1.5 mm thick CNC-laser-cut plates (5800 alu-

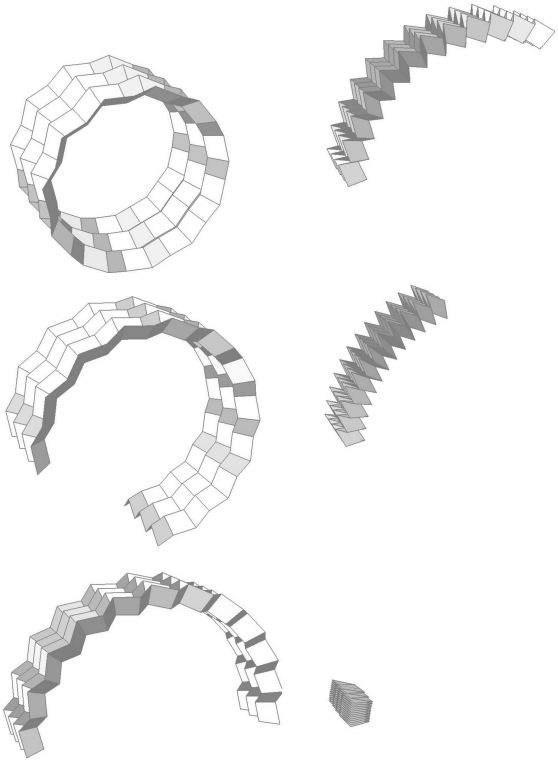

Figure 26: Concave $y$-curvature folding path

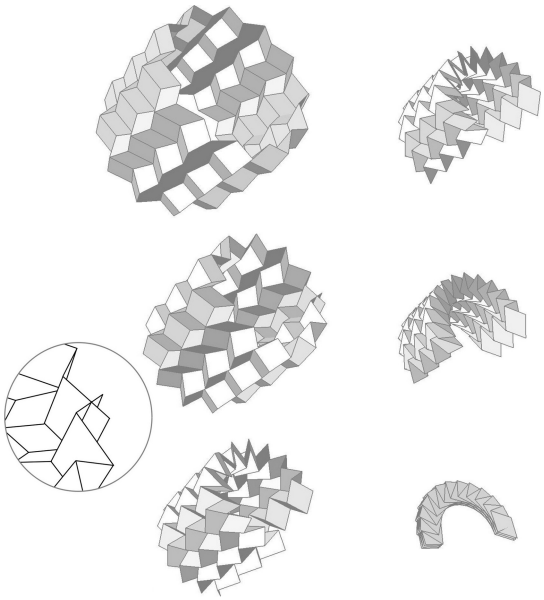

Figure 27: Concave $x$-curvature folding path with a zoom when an interpenetration occurs

minum alloy). The configuration corresponds to an $y$-curved surface with $\alpha = 67.15°$, $\beta = 19.28°$, $\gamma = 15.69°$, $l = 50.14\,\text{cm}$ and a span of approx. 278 cm.

The comparison of the model and physical realization features, for kinematics and stiffness point of view, are not under the scope of this article, but works are in progress [10].

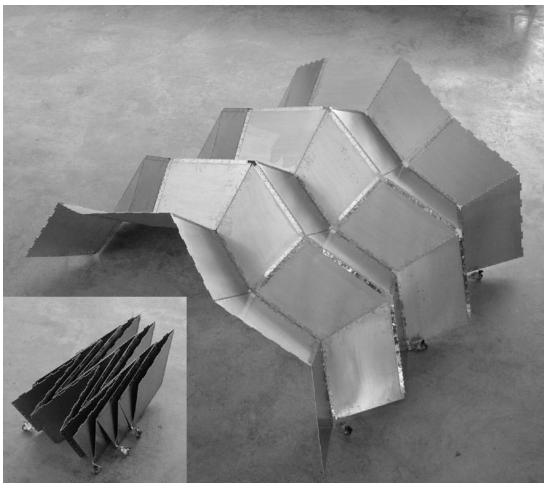

Figure 28: Physical model of a single curvature design (unfolded state, and the almost flat-folded state at the same scale)

If the design angles $\delta$ or $\gamma$ are allowed to change at each raw of units, one can design free-form single curved corrugated surfaces still foldable and unfoldable, as in Figure 29. This is performed with the additional complexity of non-repetitive units.

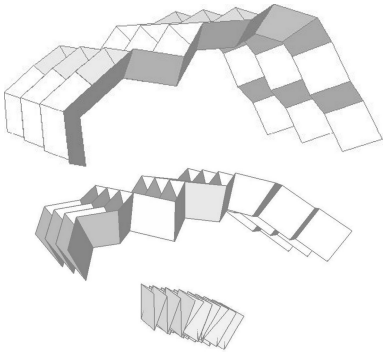

Figure 29: Free-form single curved foldable corrugated surface

# 6 Conclusions

It is possible to design, from any given bidimensional curve, a single-curved foldable / unfoldable surface that posses kinematic and structural features. In our classification those surfaces are called non-developable and flat-foldable corrugated surfaces. For these characteristics, they are suitable for application in civil engineering and architecture, for instance for the construction of temporary structures or convertible roofs, if we substitute the plates with thick panels, linear hinges with waterproof mechanical articulations, and by using actuators to drive the one-degree-of-freedom folding movement. From a geometrical point of view we observed the phenomenon of interpenetration of plates in the folding motion of two curved configurations, confirming that the local conditions of foldability do not necessarily lead to the global foldability, that requires both the existence of folding movement and no interpenetration of plates. Assessing the corrugated surface stiffness, from a simulation point of view with finite elements, as well as experimentally on a mockup of such a structure are currently under work.

**Acknowledgments.** The first author acknowledges funding from the 2010 Erasmus Exchange Program. The authors wish to thank Pr. F. Krasucki and Pr. S. Lenci for their engagement in developing this work in the framework of Erasmus program.

# References

[1] H. U. Buri and Y. Weinand. Die provisorische Kapelle von St. loup. *Bulletin Schweizerische Arbeitsgemeinschaft für Holzforschung*, (2):16–20, 2008.

[2] J. H. Cantarella, E. D. Demaine, H. N. Iben, and J. F. O'Brien. An energy-driven approach to linkage unfolding. In *20th Annual Symposium on Computational Geometry*, pages 134–143, Brooklyn, New York, 2004.

[3] B. Dacorogna, P. Marcellini, and E. Paolini. Lipschitz-continuous local isometric immersions: Rigid maps and origami. *Journal de Mathématiques Pures et Appliquées*, 90(1):66–81, 2008.

[4] B. Dacorogna, P. Marcellini, and E. Paolini. Origami and partial differential equations. *Notices of the American Mathematics Society*, 57(5):598–606, 2010.

[5] J.-M. Delarue and J.-F. Brossin. Figuration graphique et recherche structurale. Constructions plissées. Technical Report 411/87, École Nationale Supérieure d'Architecture de Paris-Villemin, 1986.

[6] E. D. Demaine, M. L. Demaine, V. Hart, G. N. Price, and T. Tachi. (Non)existence of pleated folds: How paper folds between creases. In *7th Japan Conference on Computational Geometry and Graphs*, Kanazawa, Ishikawa, Japan, November 11-13 2009. To appear (available at http://arxiv.org/abs/0906.4747).

[7] E. D. Demaine and J. O'Rourke. *Geometric Folding Algorithms: Linkages, Origami, Polyhedra*. Cambridge University Press, New York, USA, 2008.

[8] J. L. Duncan, J. P. Duncan, R. Sowerby, and B. S. Levy. Folding without distortion: Curved-line folding of sheet metal. *Sheet Metal Industries*, 58(7):527–533, 1981.

[9] D. Dureisseix. An overview of mechanisms and patterns with origami. *International Journal of Space Structures*, to appear.

[10] D. Dureisseix, F. Gioia, R. Motro, and B. Maurin. Conception d'une enveloppe plissée pliable-dépliable. In *Proceedings of the 10e Colloque National en Calcul des Structures — CSMA2011*, Giens, France, may 2011.

[11] A. El Smaili and R. Motro. Foldable / unfoldable curved tensegrity systems by finite mechanism activation. *Journal of the International Association for Shell and Spatial Structures*, 48(3):153–160, 2007.

[12] C. Hoberman. Curved pleated sheet structures, 1993. US Patent 5234727.

[13] D. A. Huffman. Curvature and creases: a primer on paper. *IEEE Transactions on Computers*, C-25(10):1010–1019, 1976.

[14] T. Hull. *Project Origami*. A K Peters, 2006.

[15] G. W. Hunt and I. Ario. Twist buckling and the foldable cylinder: an exercise in origami. *International Journal of Non-Linear Mechanics*, 40(6):833–843, 2005.

[16] K. Ikema, A. V. Gubarevich, and O. Odawara. Deformation analysis of a joint structure designed for space suit with the aid of an origami technology. In *27th International Symposium on Space Technology and Science (ISTS)*, Tsukuba, 2009.

[17] M. Kilian, S. Flöry, Z. Chen, N. J. Mitra, A. Sheffer, and H. Pottmann. Curved folding. *ACM Transactions on Graphics*, 27(3):1–9, 2008.

[18] D. Koschitz, E. D. Demaine, and M. L. Demaine. Curved crease origami. In *Advances in Architectural Geometry*, pages 29–32, Vienna, Austria, September 13-16 2008.

[19] K. Miura. Method of packaging and deployment of large membranes in space. *The Institute of Space and Astronautical Science report*, 618:1–9, 1985.

[20] K. Miura. The science of Miura-ori: A review. In R. J. Lang, editor, *4th International Meeting of Origami Science, Mathematics, and Education*, pages 87–100. A K Peters, 2009.

[21] K. Miura and S. Pelligrino. Structural concepts and their theoretical foundations. Unpublished booklet, 2001.

[22] F. Otto, R. Trostel, and F. K. Schleyer, editors. *Tensile structures; design, structure, and calculation of buildings of cables, nets, and membranes*, volume 1 and 2. The MIT Press, Cambridge, MA, 1973.

[23] J. E. Shigley and J. J. Uicker. *Theory of Machines and Mechanisms*. McGraw-Hill, New York, 2nd edition, 1995.

[24] I. Stotz, G. Gouaty, and Y. Weinand. Iterative Geometric Design for Architecture. *Journal of the International Association for Shell and Spatial Structures*, 50(1):11–20, 2009.

[25] T. Tachi. Generalization of rigid-foldable quadrilateral-mesh origami. *Journal of the International Association for Shell and Spatial Structures*, 50(3):173–179, 2009.

[26] T. Tachi. Geometric considerations for the design of rigid origami structures. In *International Association for Shell and Spatial Structures (IASS) Symposium, Spatial Structures — Permanent and Temporary*, pages 771–782, Shanghai, China, November 2010.

[27] M. Trautz and A. Künstler. Deployable folded plate structures folding patterns based on 4-fold-mechanism using stiff plates. In A. Domingo and C. Lazaro, editors, *Proceedings of the International Association for Shell and Spatial Structures (IASS) Symposium 2009*, Valencia, 2009.

[28] W. Wu and Z. You. Modelling rigid origami with quaternions and dual quaternions. *Proceedings of the Royal Society A*, 466(2119):2155–2174, 2010.

[29] Z. Wu, I. Hagiwara, and X. Tao. Optimization of crush characteristics of the cylindrical origami structure,. *International Journal of Vehicle Design*, 43:66–81, 2007.